Analyst

Accepted Manuscript

ROYAL SOCIETY OF CHEMISTRY

www.rsc.org/analyst

An efficient signal-on aptamer-based biosensor for adenosine triphosphate detection using graphene oxide as both electrochemical and Electrochemiluminescence signal indicator

Xiang Huang,‡[a] Yuqin Li,‡[b] Xiaoshan Zhang,[c] Xin Zhang,[a] Yaowen Chen[c] and Wenhua Gao*[ac]

[a] Department of Chemistry, Shantou University, Shantou, Guangdong 515063, P. R. China.

[b] Department of Pharmacy, Taishan Medicine College, Taian, Shandong 271016, P. R. China.

[c] Analysis & Testing Center, Shantou University, Shantou, Guangdong 515063, P. R. China.

** Corresponding author. Tel: +86-22-86502774; Fax: +86-22-82903941*

E-mail address: whgao@stu.edu.cn

‡ Both the authors contributed to the paper equally.

Abstract

An efficient aptasensor was developed in which graphene oxide (GO) was employed as an indicator for both electrochemical impedance spectroscopy and electrochemiluminescence (ECL) signal generation. The aptasensor was fabricated by self-assembling the ECL probe of thiolated adenosine triphosphate binding aptamer (ABA) tagged with Ru complex ($Ru(bpy)_3^{2+}$ derivatives) onto the surface of gold nanoparticles (AuNPs) modified glassy carbon electrode (GCE). ABA immobilized onto AuNPs modified GCE could strongly adsorb GO due to the strong π-π interaction between ABA and graphene oxide, ECL quenching of the Ru complex then takes place because of energy transfer and electron transfer, and a large increase of the electron transfer resistance (R_{et}) of the electrode. While, in the presence of target adenosine triphosphate (ATP), the ABA prefers to form ABA-ATP bioaffinity complexes, which have weak affinity to graphene oxide and keep the graphene oxide away from electrode surface, thus allowing the ECL signal enhancement, and in conjunction with the decrease of the R_{et}. Because of the high ECL quenching efficiency, unique structure, and electronic properties of graphene oxide, the R_{et} and ECL intensity versus the logarithm of ATP concentration was linear in the wide range from 10 pM to 10 nM with an ultra-low detection limit of 6.7 pM, 4.8 pM, respectively. The proposed aptasensor exhibited excellent reproducibility and stability, outstanding selectivity, and ATP could be effectively distinguished from its analogues. More significantly, this efficient ECL aptasensor strategy based on GO as both electrochemical and ECL signal indicator is general and can be easily extended to other biological binding events.

Keywords: Graphene oxide; Electrochemical impedance spectroscopy; Electrochemiluminescence; Aptasensor; ATP;

Introduction

Adenosine triphosphate (ATP) is generally acknowledged as "energy currency" in most animate beings, and plays an important role in many biological processes such as regulating cellular metabolism and biochemical pathways.[1-3] The dissipative rate and concentration of ATP are closely related to common diseases such as hypoxia, hypoglycemia, Parkinson's disease and some malignant tumors.[4-6] Obviously, exploring a reliable and sensitive strategy for specific detection of ATP is not only of research interest but of practical implications in modern scientific research.

Aptamers, which are nucleic acid macromolecules of single-stranded DNA/RNA oligonucleotides, could bind with a wide array of targets with high affinity and specificity.[7-8] They are originated from large random-sequence nucleic acid libraries via an in vitro evolution process called SELEX (Systematic Evolution of Ligands by Exponential Enrichment).[9-10] Moreover, the properties of simple synthesis, excellent stability and superior sensitivity make aptamers a suitable analytical agent in many medical diagnoses.[11-13] With these advantages, numerous aptamer-based analytical methods including electrochemiluminescent (ECL),[14-18] electrochemical,[19-20] fluorescent,[21] and colorimetric [22] strategies have thus been wildly developed to detect ATP, and showed good selectivity.

Compared with other approaches, electrochemicluminescence (ECL) combines the advantages of chemiluminescence and electrochemistry, such as low back-ground signal, being easily controlled and low detection limit.[23-25] Combination of these advantages and the specific property of aptamers allows ECL to become an important and promising method in aptamer biosensors. Specially, due to their excellent stability and high luminescence efficiency, the ECL biosensors based on $Ru(bpy)_3^{2+}$/TPrA system have been mostly studied.[26-27] Particularly, the ECL biosensors based on the quenching or enhancement of $Ru(bpy)_3^{2+}$/TPrA ECL system have been extensively investigated with improved performance.[28-30] For example, using the quenching mechanism of the $Ru(bpy)_3^{2+}$/ TPrA ECL system by ferrocene[31-33] and phenol,[34-36] a novel ECL quenching mechanism in complementary oligonucleotide or aptamer based

system have been developed, and applied in specific DNA,[31-36] ATP detection.[37-38] However, efforts are still being made to develop new assay to transform the aptamer-target recognition events to chemically detectable signals, that has driven the search for new methods or material that could quench or enhance the ECL of $Ru(bpy)_3^{2+}$/ TPrA to develop new ECL-based applications, which is the key to further realize their potential in analytical applications.

Graphene oxide (GO),[39] which are heavily oxygenated, as they are decorated mostly with hydroxyl and epoxy groups on their basal planes, in addition to carboxyl, carbonyl, phenol, lactone, and quinone groups located at the sheet edges. Because of its rich physical and chemical, optical, and mechanical properties, GO has been widely used for sensitive and selective detection of various biomolecules including small molecules, metal lion, nucleic acids, and proteins.[40-42] These methods utilized three important properties of GO. First, GO is an insulating and disordered analog of highly conducting crystalline graphene.[43] Second, GO can strongly adsorb single-stranded DNA (ss-DNA) via π-stacking interaction between the ring structures in the nucleobases and the hexagonal cells of GO, while double-stranded DNA (dsDNA) cannot be adsorbed due to its more rigid structure.[44] Third, GO is a super-quencher to a wide range of fluorophores via fluorescence resonance energy transfer or nonradiative dipole-dipole coupling.[45-47] Significantly, besides the above unique properties, for the first time, we found that GO is also a quencher to $Ru(bpy)_3^{2+}$/TPrA ECL system due to energy transfer and electron transfer, and realized the high sensitive detection of specific DNA sequence.[48] It demonstrated that the oxygen-containing groups and poor electrical conductivity of GO, along with the distance between GO and $Ru(bpy)_3^{2+}$ was suggested as the reasons for quenching ECL. And the mechanism of this ECL quenching is clearly dependent on the electrochemical oxidation of phenol in the presence of aqueous media, which leading to the formation of a quenching species upon oxidation, for example, p-benzoquinone. Since benzoquinone is known to quench excited states ($Ru(bpy)_3^{2+*}$) of transition-metal complexes via energy transfer.[49]

Therefore, herein, a novel signal-on biosensor based on ATP-induced structure

switching of aptamer is developed using GO as an indicator for both electrochemical and ECL signal generation. As illustrated in scheme 1. The adenosine triphosphate binding aptemer (ABA) was used as the probe DNA, in which one end was labeled with Ru complex ($Ru(bpy)_3^{2+}$) as an ECL element, and the other end was covalently immobilized on AuNPs modified GCE via the Au-S chemistry. The ABA can strongly adsorb GO due to the strong π-π interaction between GO and ABA, resulting in a large decrease of the ECL signal, and in conjunction with a large increase of the electron transfer (R_{et}) of the electrode. While, in the presence of target ATP, the ABA preferred to form ATP-aptamer complex in lieu of aptamer-GO interaction, resulting in the GO released from the electrode surface, thus leading the enhancement of ECL signal and the decrease of R_{et}.[50] The ECL intensity and R_{et} were proportionally correlated with the concentration of the target ATP, whereby allowing the quantitative detection of ATP. Here, the electron transfer (R_{et}) resistance on the GO treated electrode surface was monitored by using electrochemical impedance spectroscopy (EIS) to compare the results from the ECL quenching of GO. The designed aptasensor exhibited excellent performance, and has been successfully applied in the direct detection of ATP in human serum samples and possessed its practical application in bioanalysis and clinical diagnosis.

Experimental

Chemical and Materials

The ATP-binding aptamer (ABA): 5'-SH-$(CH_2)_6$-ACCTGGGGGAGTATTGGGGGAGGAAGGT-$(CH_2)_6$-NH_2-3′ and adenosine triphosphate (ATP), cytosine triphosphate (CTP), guanosine triphosphate (GTP), thymidine triphosphate (TTP), and uridine triphosphate (UTP) were all purchased from the Sangon biotech Co., Ltd. (Shanghai, China). Red cell lysis buffer (RCLB) was purchased from Beyotime Biotech Co., Ltd. (Shanghai, China). The human serum samples were obtained from infirmary of Shantou University. Tris (2,2-bipyridyl) ruthenium(II) chloride hexahydrate, 2-mercaptohexanol (MCH) were purchased from Sigma-Aldrich (St. Louis, MO, USA), tripropylamine (TPrA), 2,2'-bipyridine (bpy), N-hydroxysuccinimide ester (NHS), and tetrachloroauric(III) acid tetrahydrate [$HAuCl_4$ $4H_2O$] were obtained from Aladdin Chemical Reagent Co. Ltd. (Shanghai, China). Ruthenium (III) chloride hydrate, 2,2′-bipyridyl-4,4'-dicarboxylic acid (dcbpy), sodium hexafluorophosphate, N,N'-dicyclohexyl carbodiimide (DCC) were purchased from Sinopharm Chemical Reagent Co. Ltd. (Shanghai, China). Graphite flakes (325 mesh) was purchased from XFNANO Material Tech Co. Ltd. (Nan Jing, China). Phosphate buffered saline (PBS, pH 7.4) with different concentrations were prepared by mixing standard stock solutions 0.1 M NaH_2PO_4, 0.1 M Na_2HPO_4 and 0.1 M NaCl, then diluting with deionized water. A concentration of 10 mM phosphate buffered saline was used as incubation buffer and washing solution, and PBS (pH 7.4) containing TPrA was adjusted with phosphoric acid (H_3PO_4) or sodium hydroxide (NaOH). All other chemicals not mentioned here were of analytical reagent grade and used as received. Millipore Milli-Q water (18 MΩ cm) supplied by a Millipore Milli-Q water purification system (Bedford, MA USA) was used throughout.

Apparatus

All electrochemical measurements were performed in a conventional

three-electrode system with an IM6ex electrochemical workstation (Zahner IM6ex, Germany), using a modified GCE (3 mm in diameter) as the working electrode, a platinum wire as auxiliary electrode and Ag/AgCl electrode as reference electrode. The ECL intensity was monitored with a computerized MPI-B type ultra-weak luminescence analyzer (Xi' An Remax Electronic Science Tech. Co. Ltd. Xi' An, China) equipped with a photomultiplier. The voltage of the photomultiplier tube (PMT) was set at - 800 V.

The morphologies of nanomaterial were characterized by using a transmission electron microscope (TEM, JEM-1400, JEOL, Japan) and a scanning electron microscope (SEM, JSM-6360LA, JEOL, Japan). Ultraviolet-visible (UV-vis) absorption spectra were recorded on a Lambda 950 spectrophotometer (Perkin Elmer, USA). Atomic force microscopy (AFM) image was obtained by tapping-mode on a Nanoscope IIIa Digital Instruments with NSC15 tips (Veeco, CA, USA). X-ray diffraction (XRD) patterns was performed with a D8-Advance X-ray diffractometer (Bruker, Germany) operation using Cu Kα radiation.

Electrode cleaning, pretreatment and electrochemical deposition of AuNPs.

Prior to sensor fabrication, the GCE, with 3 mm in the diameter, was polished to a mirror using 0.3 and 0.05 μm α-Al_2O_3 slurry on a polishing cloth, respectively, following by ultrasonic cleaning with deionized water, absolute ethanol, and distilled water for 5 min, then followed by electrochemical pretreated by consecutively cycling the potential between - 1.0 V and 1.0 V at scan rate of 50 mV s^{-1} in 0.5 M H_2SO_4 solution until a reproducible cyclic voltammogram was obtained. Finally, it was rinsed with a copious amount of deionized water and dried in a nitrogen stream. Then the electrode was immediately used for electrochemical deposition of AuNPs.

The deposition of AuNPs was performed by immersing the polished GCE into 100 μM of $HAuCl_4$ solution in 5 mL of 0.5 M KNO_3 and applying a 5 s potential step from 1.1 to - 1.0 V according to our previously work.[51]

Synthesis of the ECL probe

Ruthenium bis(2,2′-bipyridine)-(2,2′-bipyridine-4,4′-dicarboxylic acid)-N-hydroxysuccinimide ester ([$Ru(bpy)_2$(dcbpy)NHS]) was synthesized according to our previously published protocols,[45] and directly used to mark the ABA to obtain the ECL probe of $Ru(bpy)_2$(dcbpy)-NHS-ABA (abbreviated as Ru-ABA). The Ru-ABA was characterized by UV-vis spectroscopy to verify that $Ru(bpy)_2$(dcbpy)NHS was indeed labeled on ABA(Fig. S1). More details about the synthesis and characterization of Ru-ABA can be found in supplementary information.

Preparation of ATP extracts from human serum samples

The human serum samples were used in this study. The samples were centrifuged at 1000 rpm for 5 min and washed with PBS five times, and resuspended in deionized water. Then a suitable concentration of red cell lysis buffer (RCLB) as ATP extractant was added for release of ATP from red cell. Finally, the samples were disrupted by sonication for 20 min at 0 °C. To remove the homogenate of cell debris, the lysate was centrifuged at 18000 rpm for 20 min at 4 °C. Then, the cell lysate was treated with deproteination by filtration using cutoff membranes.

Construction of the ECL Aptasensor.

The GCE modified by electrodeposited AuNPs was first washed with deionized water and immediately immersed in the 200 μL of the synthesized ECL probe (Ru-ABA) solution with a desired concentration for 12 h at 37 °C to assemble a monolayer of the ECL probe on the surface of the electrode through S-Au interaction. The aptasensor then was washed thoroughly in a stirred solution of 10 mM PBS for 20 min to remove the unlinked ECL probe. In order to block the uncovered surface of the electrode, which was immersed in 0.1 M PBS (pH 7.4, 0.1 M NaH_2PO_4/Na_2HPO_4 + 0.1 M NaCl) containing 1.0 mM 2-mercaptohexanol (MCH) solution for 1 h at room temperature, followed by rinsing with deionized water. Ultimately, the obtained aptasensor was kept at 4 °C in the dark.

Electrochemical impedance spectroscopy measurements of ATP

All electrochemical measurements were performed in the solution of 5 mM $[Fe(CN)_6]^{4-}/[Fe(CN)_6]^{3-}$ containing 0.1 M KCl. Electrochemical impedance measurements (EIS) were taken: the amplitude of the applied was 5.0 mV, whereas the oscillation potential of + 0.214 V was limited to the formal potential of the redox couple $[Fe(CN)_6]^{3-/4-}$ over the frequency range of 1 Hz to 100000 Hz. Randle equivalent circuit was used to fit the obtained impedance spectra, represented as a Nyquist plot in the complex plane. The concentration of ATP was quantified by the semicircle diameter, which equals the electron transfer resistance (R_{et}) of the electrode interface. All measurements were carried out at room temperature. Quantification of the ATP was based on the ΔR_{et} ($\Delta R_{et} = R_{blank}-R_{et}$), where R_{blank} and R_{et} are the R_{et} value before and after exposure to ATP solution.

ECL measurements of ATP

In a typical test, the as-prepared atpasensor was incubated with target ATP of different concentrations for 2 h at 37 °C, followed by thoroughly washing with 10 mM PBS to remove unbound ATP. Then, the ECL measurements were carried out under scanning from 0.2 V to 1.25 V at 100 mV s^{-1} in 0.1 M PBS (pH 7.4, 0.1 M NaH_2PO_4/Na_2HPO_4 + 0.1 M NaCl) containing 0.1 M TPrA with a photomultiplier tube voltage of - 800 V. Quantification of the target was based on the ECL peak intensity changes, ΔI_{ECL} ($\Delta I_{ECL} = I - I_0$), where I_0 and I are the ECL peak intensity before and after exposure to ATP solution, respectively.

Results and Discussion

Characterization of the as-synthesized GO and AuNPs modified GCE

GO was synthesized from graphite flakes by a modified Hummer's method,[52] which was confirmed by XRD, TEM and AFM, respectively. The XRD patterns of natural graphite powder and exfoliated GO were recorded in Fig. 1A. Compared with the natural graphite powder, the feature diffraction peak of exfoliated GO appears at

9.46°, corresponding to (001) reflection with a d-spacing of 0.934 nm, which is larger than d-spacing (0.337nm) of natural graphite at 26.4° due to the intercalated water molecules between layers,[53] indicating that the complete oxidation of graphite. Fig. 1B was the transmission electron microscopy (TEM) image of GO, and it clearly shows that flake like shapes of GO with sharp edges and wrinkles. The AFM image shows that the monodisperse thickness of the nanosheets was about 1.1 nm (Fig. 1C), and the lateral size is on the order of micrometres, which consistent with the literature.[52] And the detailed results of X-ray photoelectron spectroscopy (XPS) can be seen in our previously report, which indicates a high degree of oxidation with a high oxygen loading of 30.48%.[48] In addition, the typical SEM images of bare GCE and the AuNPs uniformly deposited GCE with same geometric surface areas were characterized by SEM, as shown in Fig. 1D and E, respectively. Comparing with bare GCE, it can be clearly seen that AuNPs have been electrochemically deposited on the surface of GCE, which demonstrated the prepared biosensor platform.

The preferred position for Fig. 1

Electrochemical characterization of ATP aptasensor

Electrochemical impedance spectroscopy is an effective method for monitoring the changes in the surface features of the modified electrodes in the assembly process.[54] Therefore, it was carried out to characterize the fabrication process of the proposed ATP atpasensor in 5 mM $[Fe(CN)_6]^{4-}$/$[Fe(CN)_6]^{3-}$ containing 0.1 M KCl solution. In the Nyquist diagram, the semicircle portion at higher frequencies corresponds to the electron transfer limited process, and the linear portion at lower frequencies represents the diffusion limited process. The semicircle diameter equals the electron transfer resistance, R_{et}.[55] The characteristic of EIS of different modified electrodes are shown in Fig. 2A. And, the equivalent circuit fitting with the obtained EIS spectra has also been depicted (inset in top right of Figure. 2A) according to previous reports.[56] The bare GCE exhibits a small semicircle at high frequency. When AuNPs were electrodeposited on the surface of GCE, the electrochemical response is

close to a straight line, which was characteristic of a diffusion process. When ECL probe (Ru-ABA) assembled onto electrode surface, a markedly increase of R_{et} was observed, owning to the fact that DNA hindered the movement of the $[Fe(CN)_6]^{4-}/[Fe(CN)_6]^{3-}$ redox probe towards the electrode surface. In the absence of ATP, a large amount of GO was adsorbed due to the strong noncovalent binging of GO with nucleobases. The adsorbed GO could highly repel the $[Fe(CN)_6]^{4-}/[Fe(CN)_6]^{3-}$ and inhibit the electron transfer, due to the negatively charged and electrical insulating properties of GO. Therefore, a large R_{et} increase was observed. However, when the biosensor electrode incubating in a certain concentration of ATP, a R_{et} decrease was observed because ATP aptesensor reacted with ATP to form stable DNA duplexes which results in very little adsorption of GO. The R_{et} changes above essentially revealed the successes of each step.

Further confirmation was also found by cyclic voltammetry (CV) in 5 mM $[Fe(CN)_6]^{4-}/[Fe(CN)_6]^{3-}$ containing 0.1 M KCl solution, as shown in Fig 2B. The CV at bare GCE showed a quasi-reversible redox reaction and a ratio of the peak currents of about 1:1. The peak current obviously increased after AuNPs were electrodeposited onto the surface of GCE, which implied that the conductive AuNPs accelerated the electron transfer. The peak current significantly decreased when the Ru-ABA was immobilized onto the surface of the AuNPs modified GCE, which probably due to the created kinetics barrier between $[Fe(CN)_6]^{4-}/[Fe(CN)_6]^{3-}$ and the negatively charged phosphate backbones of DNA. Similarly, the peak current was further decreased after adsorption of GO, since GO is an insulator. While, a relative high peak current was restored, in which the bases that could interact with GO were hidden in the presence ATP. This result is perfectly consistent with the EIS changes, thus further confirmed the successful preparation of biosensor.

The preferred position for Fig. 2

The ECL signals at each immobilization steps were also recorded to monitor the fabrication of the aptasensor in the 0.1 M PBS containing 0.1 M TPrA using a linear

potential scan technique. The corresponding ECL intensity *vs.* potential curves of the biosensor electrode were presented in Fig. 3. It can be seen that the signal was very low, even negligible, before ECL probes were assembled to the GCE via S-Au interaction. After Ru-ABA were assembled to the electrode, the ECL signal increased significantly, this proved that the signal was generated from Ru complex. However, there is no obvious ECL signal response can be found when GO was absorbed onto the ECL probe modified GCE by the strong binging ability of ABA with GO. This distinctly decrease indicated that an efficient quenching effect of GO on the ECL of $Ru(bpy)_3^{2+}$/TPrA system, as shown in Fig 3. Upon incubating in a certain concentration of ATP, the ABA preferred to form ATP-aptamer complex in lieu of aptamer-GO interaction.[50] As a result, the GO was released from the electrode surface and the ECL intensity obviously increased. In addition, shown in the inset of Fig. 3 is the ECL signal-time curve under continuous potential scanning for six cycles. The stable and high ECL signals suggested that this aptasensor is very suitably for ultrasensitive determination of ATP.

The preferred position for Fig. 3

Optimization of the detection conditions

The detection conditions were optimized by ECL measurements, the ECL intensity strongly depends on the pH of the detection solution. Thus, the influence of pH from 5.8 to 8.6 on the biosensor performance was investigated. As shown in Fig 4A, the ECL intensity of the aptasensor reached the maximum at pH 7.4. Therefore, pH 7.4 was selected for the following ECL measurements.

The incubation times greatly affected the analytical performance of the proposed biosensor. Therefore, the incubation times of the aptesensor with both GO and target ATP were further optimized. When the incubation time with GO increased, more GO was absorbed by the aptasensor, thus the quenching efficiency increased. The quenching efficiency trended to the maximum value at 75 min (Fig 4B), indicating the saturated absorption of GO, so 75 min was used for incubation of GO. Similarly, with

the increasing incubation time of the aptesensor with a concentration of ATP, the ECL intensity increased rapidly due to the less absorption of GO. And a stable and plateau ECL intensity could be achieved after 2 h (Fig 4C), which was chosen as the optimal condition.

The preferred position for Fig. 4

Analytical performance of ATP aptasensor

Under the optimal conditions, EIS measurements were firstly used to quantitatively assess the detection limit and response range of the ATP aptasensor by utilizing GO as electrochemical indicator. In the presence of ATP, the ABA formed a duplex, in which the bases that could interact with GO were hidden. Therefore, less GO was absorbed onto the modified GCE surface as the concentration of ATP increased, Fig. 5A shows that the charge transfer resistance (R_{et}) of the redox couple decreases accordingly as the concentration of ATP increased. The changes of the electron transfer resistance, ΔR_{et} ($\Delta R_{et} = R_{blank} - R_{et}$) is plotted as a function of the logarithm of ATP concentration in the range from 10 pM to 10 nM. The regression equation was $\Delta R_{et} = 1539.7 + 576.5 \lg(c_{ATP})$ (c: nM) with a regression coefficient R = 0.995 and a detection limit of 6.7 pM (Fig 5B, S/N=3). The limit of detection (LOD), which was defined as the concentration corresponding to the mean blank value plus 3 standard deviations.

The preferred position for Fig. 5

Significantly, the use of GO as an ECL quencher was investigated for ATP detection. Instead of EIS measurements, we quantitatively detect ATP by observing the ECL emission intensity of the aptasensor. According to our previously report, GO would be a well ECL quencher of TPrA/$Ru(bpy)_3^{2+}$ system, the amount of GO adsorbed onto the GCE surface was expected to directly correlated with the ECL intensity. Under the optimal conditions, the ECL intensity became large with the increasing ATP concentration because more GO released from the aptasensor surface.

As displayed in Fig 6, the calibration plot showed a good linear relationship between ECL intensity and logarithmic value of ATP concentration ranging from 10 pM to 10 nM. The equation of the calibration curve can be expressed as ΔI_{ECL} = 2262.5 + 970.8 lg(c_{ATP}) (c: nM) with a correlation coefficient of R= 0.998 (shown as the inset in Fig 6) and a detection limit of 4.8 pM (S/N=3). The LOD, which was also defined as the concentration corresponding to the mean blank value plus 3 standard deviations. Significantly, the R value a little higher than that of obtained by EIS measurements, and even the LOD slightly lower than that of the EIS approach. Moreover, the standard deviation of each point of the ratio was obviously reduced compared to the EIS results, which indicates the method observing ECL intensity is more reproducible than EIS. And the problem of reproducibility in the EIS measurements for biosensor application was consistent with the previously literature.[57] The LOD of 4.8 pM in our work is highly sensitive, which is superior to these obtained from other approaches. The comparing of detection limit of the proposed aptasensor with reported methods were presented in Table S1. Note that the sensitivity obtained for the aptasensor by utilizing the high quenching efficiency of GO in ECL of $Ru(bpy)_3^{2+}$/TPrA system.

The preferred position for Fig. 6

Stability, selectivity and reproducibility of the ATP aptasensor

The long-time stability of this ATP aptasensor is a key stability studies of the proposed aptasensor have been carried out by our group. The results indicate that, the ECL response of the aptasensor gradually decreased to approximately 93% of its original value after it had been stored in dark at 4 ˚C for one month (Fig 7A). In addition, the stability of the ECL intensity of the proposed aptasensor to various concentration of ATP was further investigated and the results were presented in Fig. 7B, it shows that the ECL intensity increased with the increasing concentration of ATP, and a stable curve at every concentration could be obtained. These results further demonstrating that the aptasensor possessed excellent stability.

The preferred position for Fig. 7

To investigate the binding specificity of the aptasensor, the ECL intensity changes upon incubation with ATP, CTP, GTP, TTP and UTP were measured under the same experimental conditions. As illustrated in Fig 8, compared with the ECL response of aptasensor towards 10 nM ATP, the proposed aptasensor did not show any significant responses towards 100 nM CTP, 100 nM GTP, 100 nM TTP and 100 nM UTP, respectively, suggesting that the above ATP analogues interfered less in the ATP detection. Furthermore, the cross-sensitivity of the aptasensor in a mixture with different interfering species containing 10 nM ATP was also examined. The signal obtained from the complex was similar to that obtained from ATP only. All these results indicated that the aptasensor was very specific for ATP determination.

The preferred position for Fig. 8

The reproducibility of the proposed aptasensor for ATP was assessed by the relative standard derivations of intra- and inter-assay precision. Which were evaluated by measuring one ATP level for 5 reduplicate measurements, and with 5 aptasensors made at the same electrode. The ECL responses of relative standard deviations (RSD) of the intra- and inter-assay obtained from 5 nM ATP were 4.2% and 5.8%, respectively, which indicate the precision and fabrication reproducibility were acceptable.

Analysis of ATP in human serum samples

To explore whether the developed aptasensor could be applied in real complex sample analysis, four serum samples were diluted with the appropriate volumes of 0.1 M PBS and then a recovery experiment of the aptasensor was carried out. The serum samples were spiked with 1.0, 2.0, 5.0 and 10.0 nM ATP, then detected by the proposed ECL aptasensor, respectively. The results are shown in Table S2, the recoveries are between 96.0% and 107.5%, and the RSDs are in the range of 4.18% to 6.12%, which suggests the proposed biosensor can be successfully applied for detection of ATP in the complex real samples.

More significantly, for further demonstrate the proposed aptasensor was applicable to real samples, we applied this sensor to detect the ATP in human serum directly. The results of the determination were shown in Table S3 and Fig S2. The detected concentration determination of ATP in the human serum was about 0.33 nM. Meanwhile, the stable and high ECL response suggested that the proposed aptasensor was suitable for real ATP concentration detection.

Conclusions

In conclusions, an efficient sensing strategy for ATP detection by taking advantages of the unique electrical insulation property and high ECL quenching ability of GO, the unique GO/aptamer interaction and the specific aptamer-target recognition. The designed ECL aptasensor exhibited excellent performances and ATP could be effectively discriminated from its analogues. ATP has also been determined in diluted human serum samples with satisfactory results, indicating the applicability of this assay. In addition, the charge transfer resistance (R_{et}) on the GO treated electrode surface was also monitored by using electrochemical impedance spectroscopy (EIS) to compare the results from the ECL quenching of GO, which demonstrated that the performances obtained by ECL could be superior to that of obtained by EIS in the same aptasensor system. More significantly, this proposed sensing strategy could be easy to generalize this aptamer-based strategy to detect a spectrum of targets using GO as an ECL quencher and different functional DNA or RNA structures.

Acknowledgements

We are grateful for the financial support from the Natural Science Foundation of Guangdong Province (No. S2011010005208 & No. 2014A030313480), the Science & Technology Project of Guangdong Province (No. 2013B030600001) and the Guangdong High Education Fund of Science and Technology Innovation (No. 2013KJCX0078).

Reference

1 S. Zhang, Y. Yan and S. Bi, *Anal. Chem*., 2009, **81**, 8695-8701.

2 X. Yan, X. Cui and L. S. Li. *J. Am. Chem. Soc*., 2010, **132**, 5944-5945.

3 E. H. Abraham, K. M. Sterling, R. J. Kim, A. Y. Salikhova, H. B. Huffman, M. A. Crockett, N. Johnston, H. W. Parker, W. E. Boyle, A. Hartov, E. Demidenko, J. Efird, J. Kahn, S. A. Grubman, D. M. Jefferson, S. C. Robson, J. H. Thakar, A. Lorico, G. Rappa, A. C. Sartorelli and P. Okunieff, *Blood Cells, Mol., Dis*., 2001, **27**, 165-180.

4 J. A. Cruz-Aguado, Y. Chen, Z. Zhang, N. H. Elowe, M. A. Brook and J. D. Brennan, *J. Am. Chem. Soc*., 2004,**126**, 6878-6879.

5 L. Annunziato, G. Pignataro and G. F. Di Renzo, *Pharmacol. Rev*., 2004, **56**, 633-654.

6 A. V. Gourine, E. Llaudet, N. Dale and K. M. Spyer, *Nature*., 2005, **436**, 108-111.

7 E. J. Cho, J. W. Lee and A. D. Ellington, *Ann Rev Anal Chem*., 2009, **2**, 241-264.

8 X. B. Yin, *Trac-Trend Anal Chem*., 2012, **33**, 81-94.

9 C. Tuerk and L. Gold, *Science*., 1990, **249**, 505-510.

10 A. D. Ellington and J. W. Szostak, *Nature*., 1990, **346**, 818-822.

11 D. Li, S. Song and C. Fan, *Acc. Chem. Res*., 2010, **43**, 631-641.

12 J. Zhang, L. H. Wang, D. Pan, S. P. Song, F. Y. C. Boey, H. Zhang and C. H. Fan, *Small.*, 2008, **4**, 1196-1200.

13 C. Y. Tian, J. J. Xu and H. Y. Chen, *Chem. Commun*., 2012, **48**, 8234-8236.

14 Z. Y. Lin, F. Luo, Q. D. Liu, L. F. Chen, B. Qiu, Z. W. Cai and G. N. Chen, *Chem. Commun*., 2011, **47**, 8064-8066.

15 Z. Y. Liu, W. Zhang, L. Z. Hu, H. J. Li, S. Y. Zhu and G. B. Xu, *Chem-Eur J*., 2010, **16**, 13356-13359.

16 J. J. Lu, M. Yan, L. Ge, S. G. Ge, S. W. Wang, J. X. Yan and J. H. Yu, *Biosens. Bioelectron*., 2013, **47**, 271-277.

17 D. Zhu, X. Zhou and D. Xing, *Biosens. Bioelectron*, 2010, 26, 285-288.

18 D. Zhu, X. Zhou and D. Xing, *Anal Chim Acta*, 2012, **725**, 39-43.

19 B. C. Yin, Y. M. Guan and B. C. Ye, *Chem. Commun*., 2012, **48**, 4208-4210.

20 B. Q. Liu, Y. L. Cui, D. P. Tang, H. H. Yang and G. N. Chen, *Chem. Commun*., 2012, **48**, 2624-2626.

21 M. Zhang, S. M. Guo, Y. R. Li, P. Zuo and B. C. Ye, *Chem. Commun*., 2012, **48**, 5488-5490.

22 H. Liang, H. X. Ouyang and Z. L. Jiang, *Analyst*., 2011,**136**, 4514-4519.

23 W. Miao, *Chem. Rev*., 2008, **108**, 2506-2553.

24 J. Wang, Y. Shan, W. W. Zhao, J. J. Xu and H. Y. Chen, *Anal. Chem*., 2011, **83**, 4004-4011.

25 S. Liu, J. Zhang, W. Tu, J. Bao and Z. Dai, *Nanoscale*., 2014, **6**, 2419-2425.

26 D. Xing, X. Zhou, D. Zhu, Y. Liao, W. Liu, H. Liu and Z. Ma, *Nat. protoc*., 2014, **9**, 1146-1159.

27 B. Sun, H. Qi, F. Ma, Q. Gao, C. Zhang and W. Miao, *Anal. Chem*., 2010, **82**, 5046-5052.

28 W. J. Miao, J. P. Choi, J. P and A. J. Bard, *J. Am. Chem. Soc*., 2002, **124**, 14478-14485.

29 Z. Y. Zu and A. J. Bard, *Anal. Chem*., 2001, **73**, 3960-3964.

30 S. Workman and M. M. Richter, *Anal. Chem*., 2000, **72**, 5556-5561.

31 W. D. Cao, J. P. Ferrance, J. Demas and J. P. Landers, *J. Am. Chem. Soc*., 2006, **128**, 7572-7578.

32 L. F. Chen, Q. H. Cai, F. Luo, X. Chen, X. Zhu, B. Qiu, Z. Y. Lin and G. N. Chen, *Chem. Commun*., 2010, **46**, 7751-7753.

33 F. Li, Y. Yu, Q. Li, M. Zhou and H. Cui, *Anal. Chem*., 2014. **86**, 1608-1613.

34 J. McCall, C. Alexander and M. M. Richter, *Anal. Chem*., 1999, **71**, 2523-2527.

35 J. McCall and M. M. Richter, *Analyst*., 2000, **125**, 545-548.

36 X. Tang, D. Zhao, J. He, F. Li, J. Peng and M. Zhang, *Anal. Chem.*, 2013, **85**, 1711-1718.

37 L. Chen, Q. Cai, F. Luo, X. Chen, X. Zhu, B. Qiu and G. Chen, *Chem. Commun*., 2010, **46**, 7751-7753.

38 Z. Lin, F. Luo, Q. Liu, L. Chen, B. Qiu, Z. Cai and G. Chen, *Chem. Commun*., 2011, **47**, 8064-8066.

39 D. Chen, H. Feng and J. Li, *Chem Rev*., 2012, **112**, 6027-6053.

40 C. H. Lu, H. H. Yang, C. L. Zhu, X. Chen and G. N. Chen, *Angew. Chem., Int. Ed*., 2009, **48**, 4785-4787.

41 Y. Guo, L. Deng, J. Li, S. Guo, E. Wang and S. Dong, *ACS Nano*., 2011, **5**, 1282-1290.

42 Y. Pu, Z. Zhu, D. Han, H. Liu, J. Liu, J. Liao, K. Zhang and W. Tan, *Analyst*., 2011, **136**, 4138-4140.

43 K.P. Loh, Q. Bao, G. Eda and M. Chhowalla, *Nat Chem*., 2010. **2**, 1015-1024.

44 S. He, B. Song, D. Li, C. Zhu, W. Qi, Y. Wen, L. Wang, S. Song, H. Fang and Fan, C. *Adv. Funct. Mater*., 2010, **20**, 453-459.

45 C. Zhang, Y. Yuan, S. Zhang, Y. Wang, Z. Liu, *Angew. Chem., Int. Ed*., 2011, **50**, 6851-6854.

46 D. Zhu, L. Zhang, W. Ma, S. Lu and X. Xing, *Biosens. Bioelectron*., 2015, **65**, 152-158.

47 D. Zhu, X. Xing, W. Ma, S. Lu and B. Su, *Sensor Actuat B-Chem*., 2014, 193, 178-184.

48 X. Huang, X. P. Huang, A. Zhang, B. R. Zhuo, F. S. Lu, Y. W. Chen and W. H. Gao, *Biosens. Bioelectron*., 2015, **70**, 442-446.

49 M. R. Wasieleski. *Chem. Rev.,* 1992, **92**, 435.

50 L. Wang, M. Xu, L. Han, M. Zhou, C. Zhu and S. Dong. *Anal Chem.*, 2012, **84**(17), 7301-7307.

51 W. H. Gao, A. Zhang, Y. W. Chen, Z. G. Chen, Y. W. Chen, F. S. Lu and Z. Chen, *Biosens. Bioelectron*., 2013, **49**, 139-145.

52 D. C. Marcano, D. V. Kosynkin, J. M. Berlin, A. Sinitskii, Z. Sun, A. Slesarey, L. B. Alemary, W. Lu and J. M. Tour, *ACS nano*., 2010, **4**, 4806-4814.

53 D. A. Dikin, S. Stankovich, E. J. Zimney, R. D. Piner, G. H. Dommett, G. Evmenenko, S. T. Nguyen, and R. S. Ruoff, *Nature*., 2007, **448**, 457-460.

54 X. H. Li , L. Dai , Y. Liu , X. J. Chen , W. Yan , L. P. Jiang and J. J. Zhu , *Adv. Funct. Mater*., 2009, **19**, 3120-3128.

55 J. J. Zhu, L. L. Li, K. P. Liu, G. H. Yang, C. M. Wang and J. R. Zhang, *Adv. Funct.*

Mater., 2011, **21**, 869-878.

56 X. Chen, Y, Wang, J. Zhou, W. Yan, X. Li and J. J. Zhu, *Anal. Chem*., 2008, **80**, 2133-2140.

57 A. Bogomolova, E. Komarova, K. Reber, T. Gerasimov, O. Yavuz, S. Bhatt and M. Aldissi, *Anal. Chem*., 2009, **81**, 3944-3949.

Captions to figures

Scheme 1 Schematic diagram of the aptasensor based on GO as signal indicator for the detection of ATP.

Fig. 1 (A) XRD patterns of the pristine graphite (a) and exfoliated GO (b); (B) TEM image of GO; (C) Tapping mode AFM of exfoliated GO with height profiles, deposited on freshly cleaved mica substrates; (D) SEM images of Bare GCE; (E) AuNPs deposited onto GCE surfaces.

Fig. 2 (A): Nyquist diagram of electrochemical impedance spectra at (a) a bare GCE, (b) AuNPs/GCE, (c) Ru-ABA/AuNPs/GCE, (d) GO/ Ru-ABA/AuNPs/GCE, (e) ATP/ GO/Ru-ABA/AuNPs/GCE in the solution of 5 mM $[Fe(CN)_6]^{4-}/[Fe(CN)_6]^{3-}$ containing 0.1 M KCl. The frequency range was 1 Hz-100000 Hz with a signal amplitude of 5 mV. The inset of the top right corner shows the equivalent circuit to fit with obtained EIS spectra. (B): Cyclic voltammotrams of (a) a bare GCE, (b) AuNPs/GCE, (c) ABA-Ru/AuNPs/GCE, (d) GO/ Ru-ABA/AuNPs/GCE, (e) ATP/ GO/ Ru-ABA/AuNPs/GCE in the solution of 5 mM $[Fe(CN)_6]^{4-}/[Fe(CN)_6]^{3-}$ containing 0.1 M KCl. Scan rate: 100 mV s^{-1}.

Fig. 3 ECL intensity *vs.* potential curves for the (a) AuNPs modified GCE, (b) the AuNPs/GCE biosensor modified with Ru-ABA, (c) the Ru-ABA/AuNPs biosensor incubation with GO, (d) and then incubated with 1 nM ATP. Inset: ECL intensity vs. time curves for the aptasensor under continuous CV for six cycles. ECL curves were measured in 0.1 M PBS containing 0.1 M TPrA at 100 mV s^{-1}.

Fig. 4 Optimization of the aptasensor experiment conditions, effects of (A) pH of detection solution, (B) incubation time for GO, and (C) incubation time for ATP on ECL response of the aptasensor. ECL intensity were measured in the absence of (B) and presence (A, C) of 5 nM ATP. Error bars represent the standard deviation of three

parallel experiments.

Fig. 5 EIS response of the aptasensor with different concentration of ATP. (a) 0, (b) 10 pM, (c) 50 pM, (d) 100 pM, (e) 0.5 nM, (f) 1 nM, (g) 5 nM, (h) 10 nM. (B) The linear relationship between ΔR_{et} and logarithm of the ATP concentrations. The error bars represent the standard deviation of three parallel measurements.

Fig. 6 ECL intensity of the aptasensor with different concentration of ATP. (a) 0, (b) 10 pM, (c) 50 pM, (d) 100 pM, (e) 0.5 nM, (f) 1 nM, (g) 5 nM, (h) 10 nM. Inset: linear relationship between relative ECL intensity (ΔI_{ECL}) and logarithm of the ATP concentrations. The error bars represent the standard deviation of three parallel measurements.

Fig. 7 (A) ECL intensity of the aptasensor before and after one month in the presence of 1 nM ATP. (B): ECL stability of the proposed aptasensor to various concentrations of ATP.

Fig. 8 Selectivity of the proposed aptasensor: (a) 10 nM ATP, (b) a mixture containing 10 nM ATP, 100 nM CTP and 100 nM GTP, (c) 100 nM CTP, (d) 100 nM GTP, (e) 100 nM TTP and (f) 100 nM UTP. The error bars represent the standard deviation of three measurements.

Scheme. 1

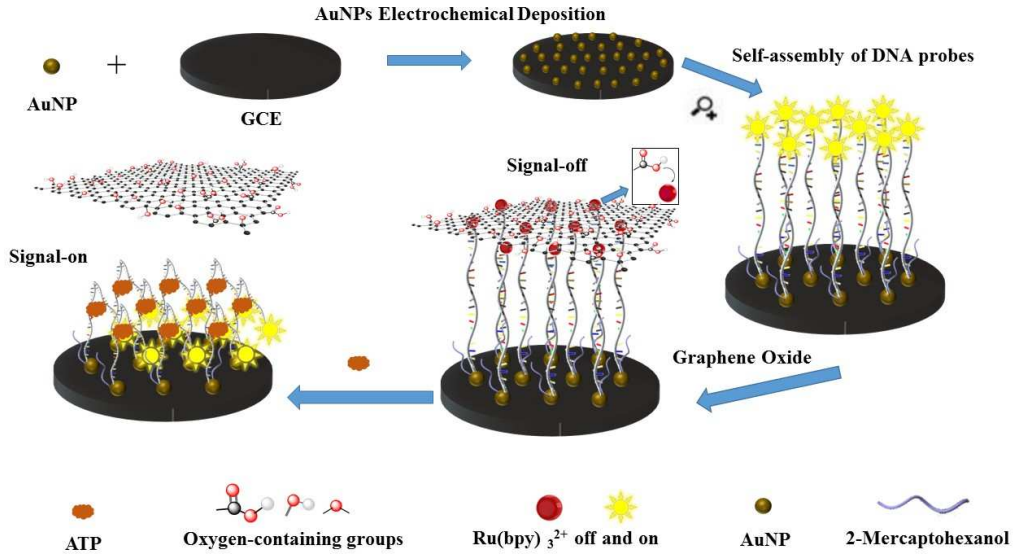

Fig. 1

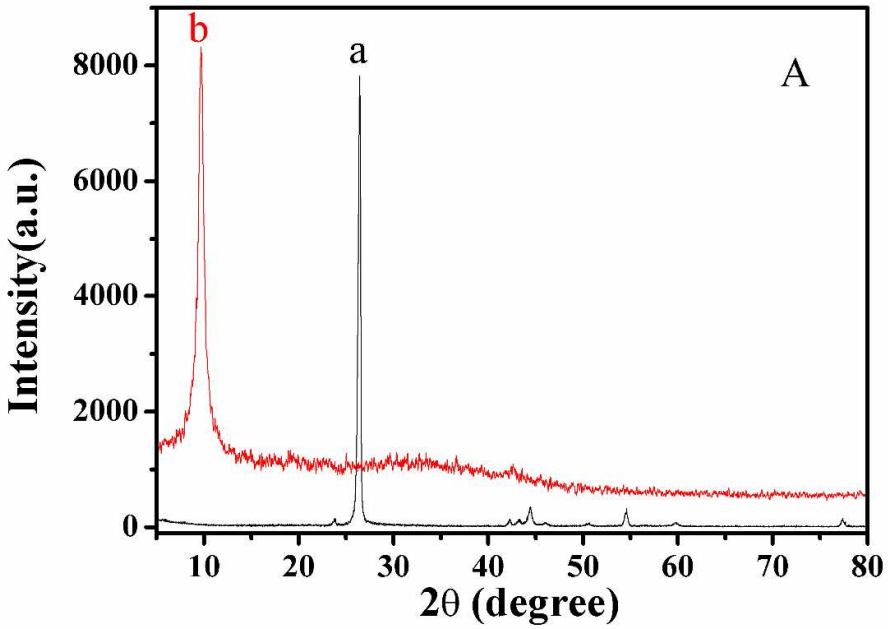

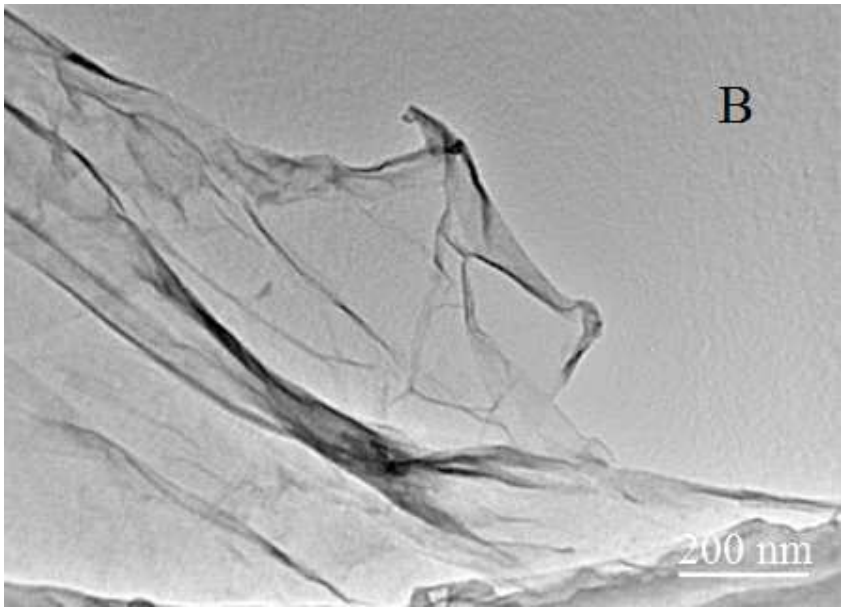

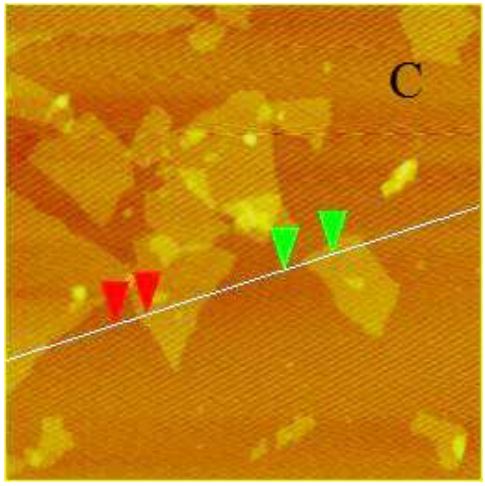

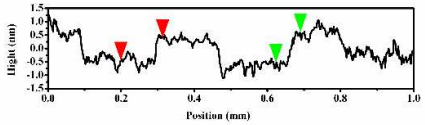

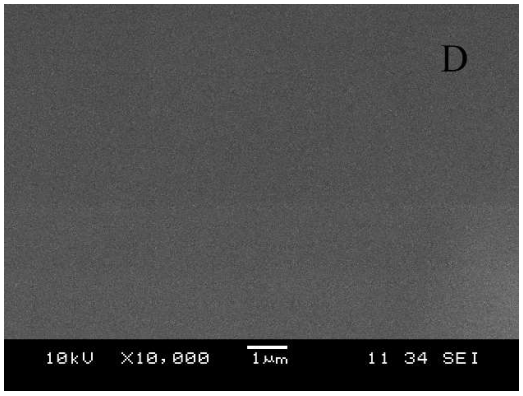

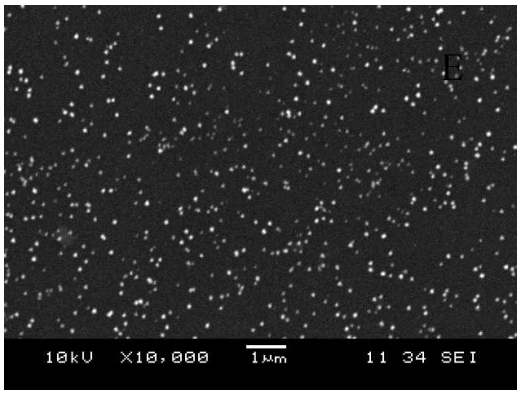

Fig. 2

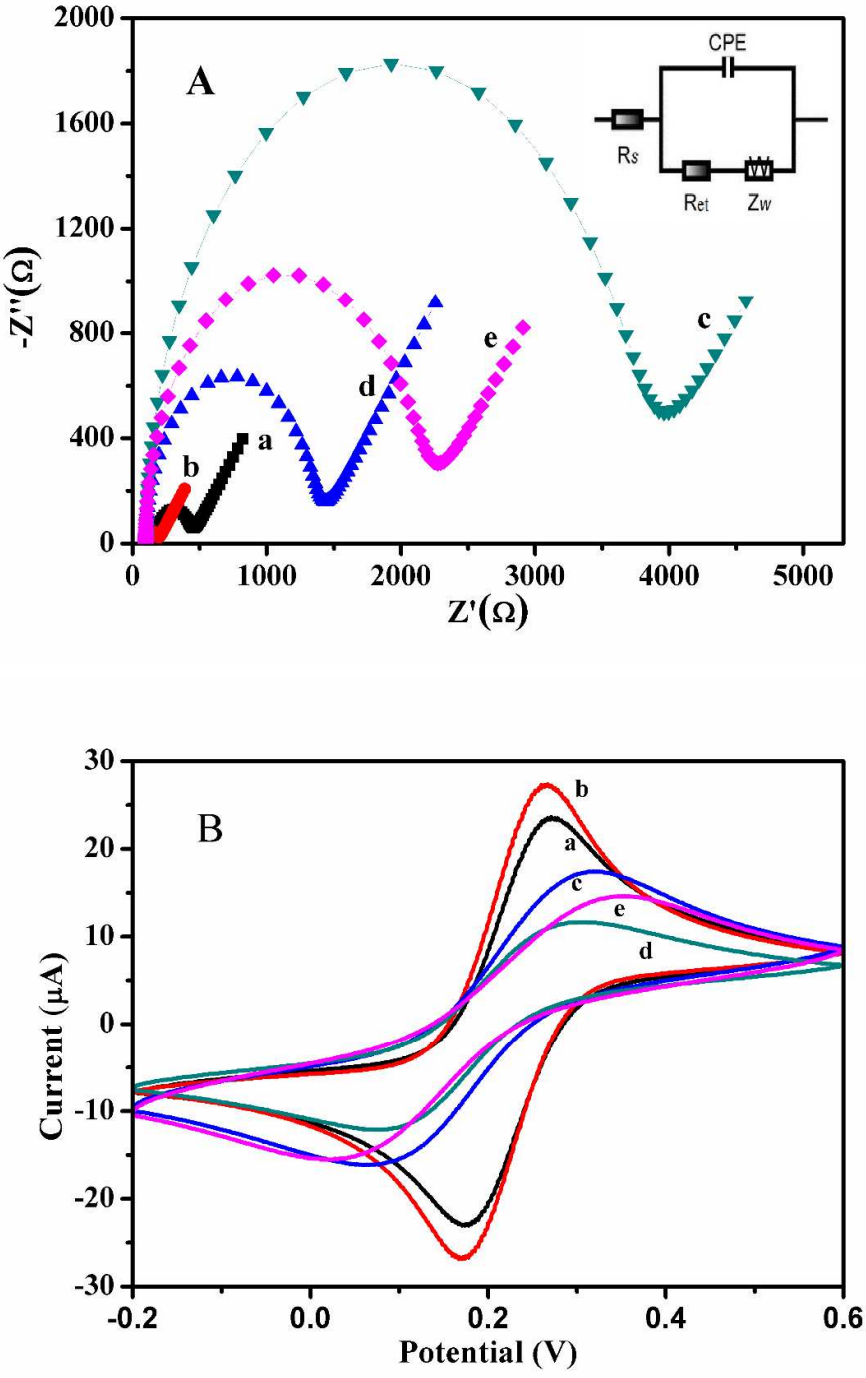

Fig. 3

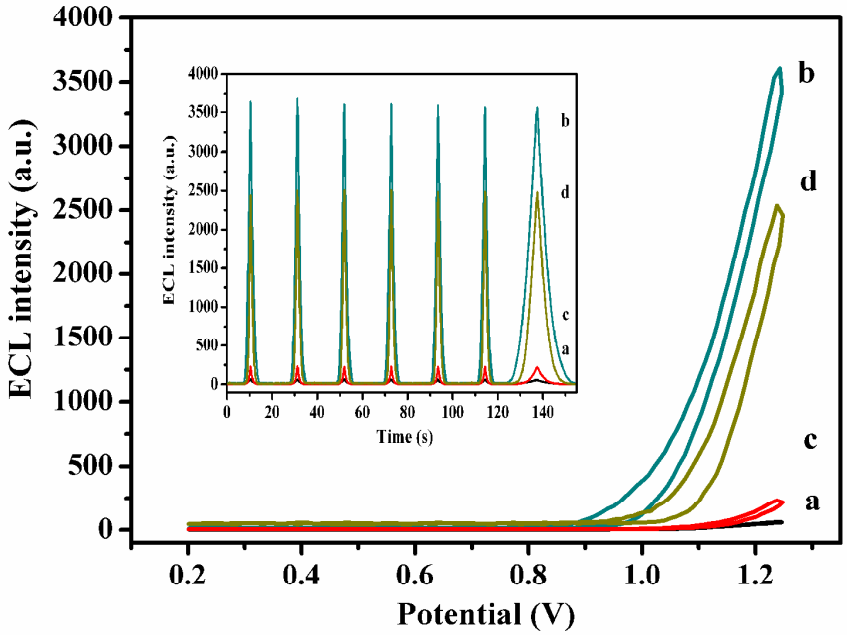

Fig. 4

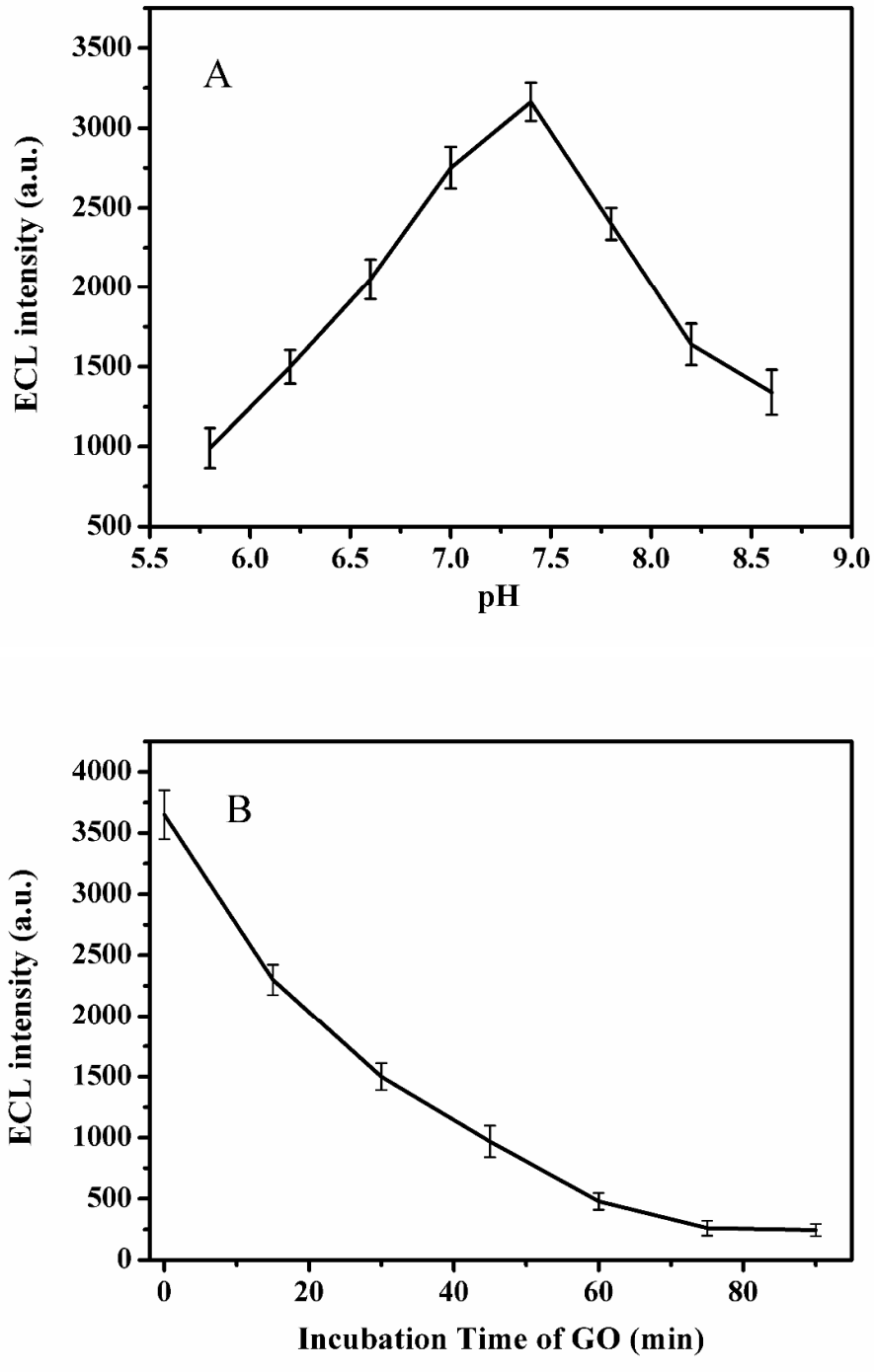

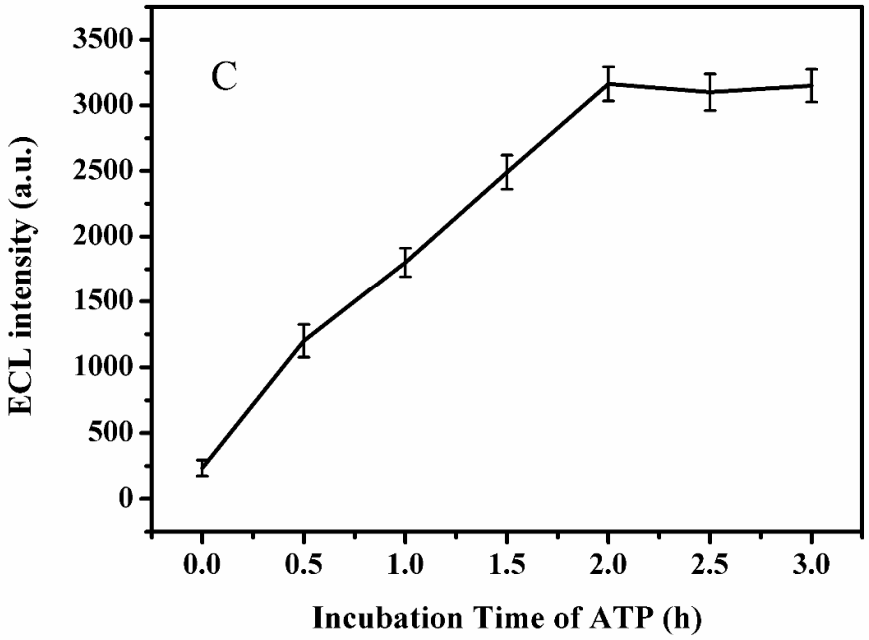

Fig. 5

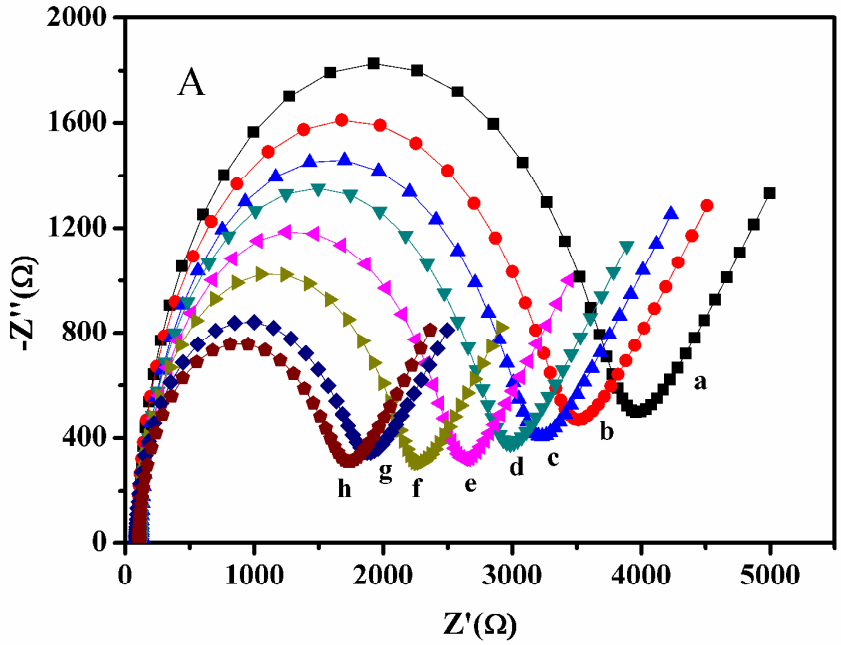

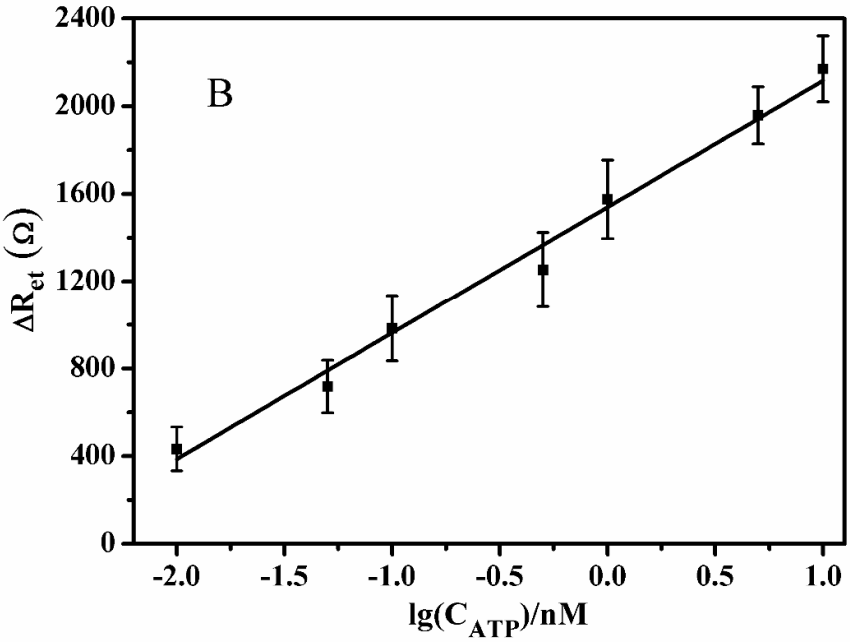

Fig. 6

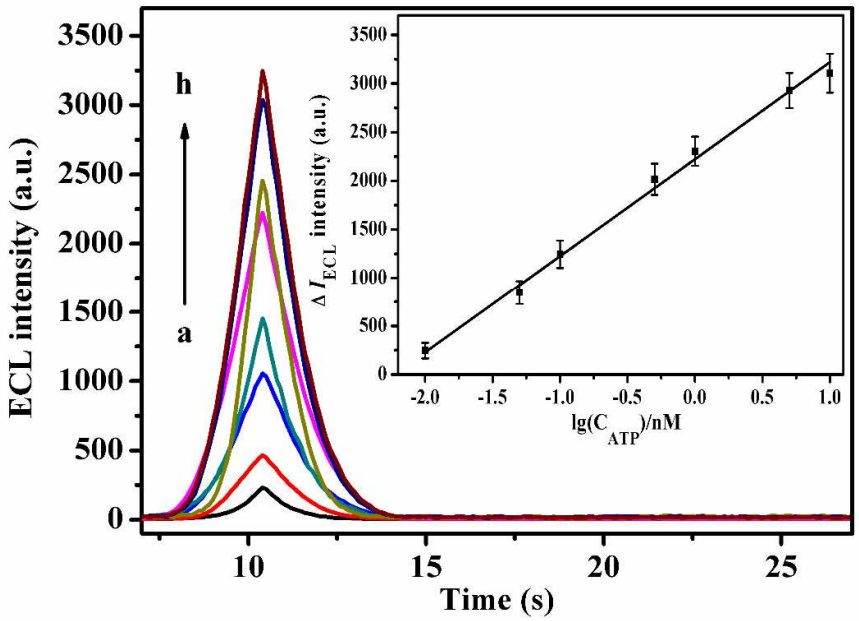

Fig. 7

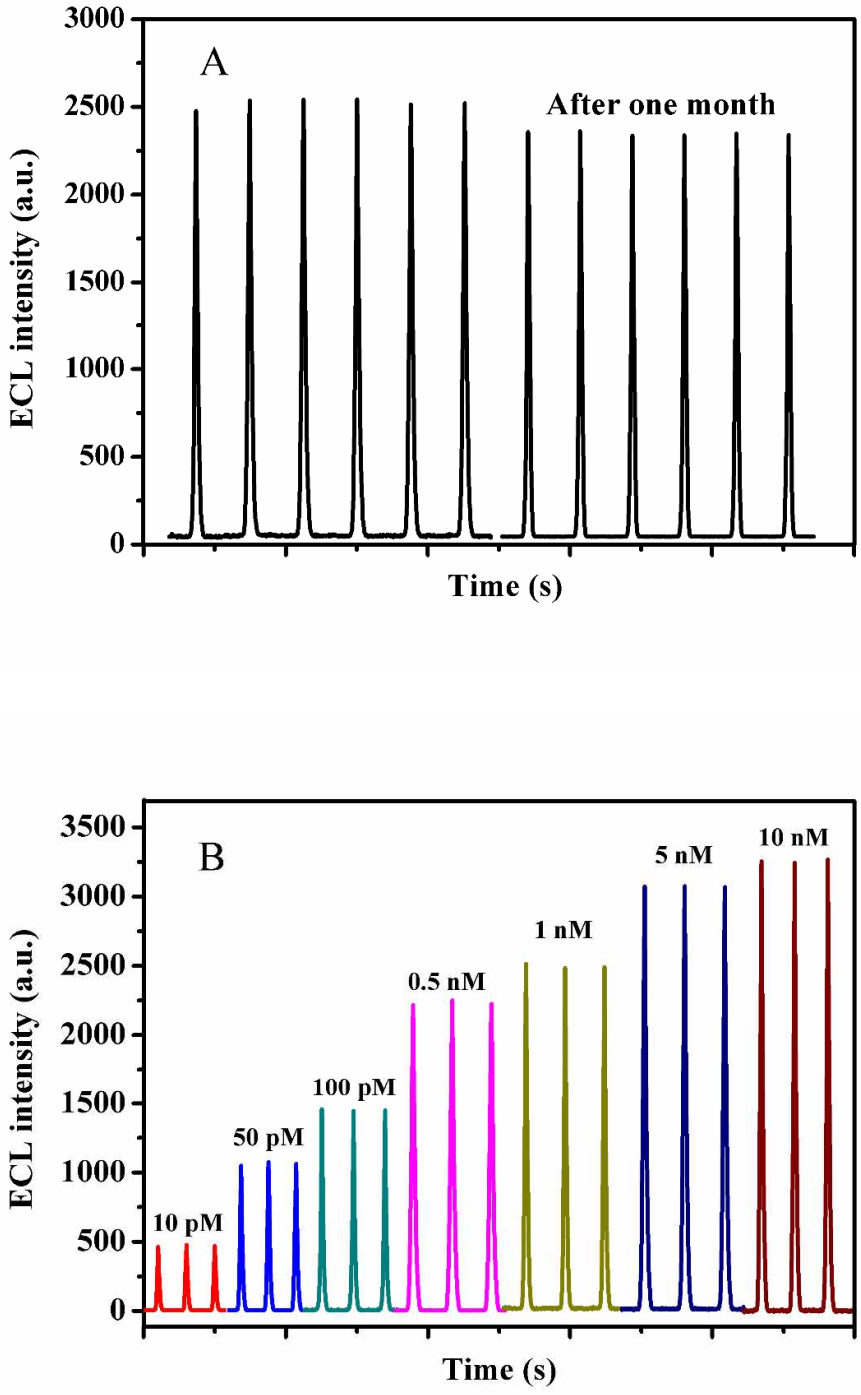

Fig. 8